Int. J. Heat Mass Transfer. Vol. 32, No. 9, pp. 1681–1695, 1989
Printed in Great Britain

0017-9310/89 $3.00 + 0.00

Mixed convection from a heated inclined plate in a channel with application to CVD

H. Q. YANG† and K. T. YANG
Department of Aerospace and Mechanical Engineering, University of Notre Dame, Notre Dame, IN 46556, U.S.A.

(*Received* 7 *July* 1988 *and in final form* 2 *February* 1989)

Abstract—A numerical study based on governing equations in skewed coordinates is made to determine the influence of forced convection on natural convection from an inclined, heated plate situated inside a horizontal channel. The forced convection is found to augment the heat transfer as well as to make the heat transfer rate more uniform on the upward-facing side of the plate. The boundary conditions, inclination angles and offset positions are found to have significant effects on the interaction of forced and natural convection.

INTRODUCTION

THE IMPORTANCE of understanding the fundamental transport phenomena and the role of fluid dynamics in chemical vapor deposition has now been well recognized [1–3]. Figure 1 shows two commonly used reactors: a horizontal reactor and a vertical reactor. The chemical vapor is supplied from the inlet and the substrate is heated by an induction coil to accelerate the reaction speed, while the reactor walls are typically cooled to minimize the particulate and impurity problem caused by deposition on the walls [3]. It is essential to have uniform film thickness and reproducible and controllable properties. The fluid dynamic behavior of horizontal reactors with $\psi = 0$ and $H = 0$ (Fig. 2) has been studied recently by various investigators [3–7]. It is realized that the condition of the reactor wall has a pronounced influence on the transfer rate through the substrate. A cooled wall, which is generally used, drives a secondary flow that is superimposed on the forced flow, remarkably modifying the transfer phenomena and causing spatial non-uniform deposition [3–6]. The entrance length for the onset of the buoyancy-driven secondary cell has been studied experimentally and numerically by Chiu and coworkers [4, 5]. It is found that the buoyancy-induced roll cells can take two forms. One is in the form of transverse rolls with axes perpendicular to the forced flow but parallel to the horizontal surface. The second is in the form of longitudinal rolls with axes parallel to the forced flow direction. The forced convection is found to suppress the initiation of the transverse rolls, but has no influence on that of the longitudinal rolls [5]. In this sense, once the Rayleigh number is higher than the critical value for Rayleigh–Bénard convection in a horizontal reactor, the longitudinal rolls will set up. The appropriate control of the secondary cell in the chemical vapor deposition process is obviously a challenging problem. In practice, the uniformity of the deposition rate may be increased by reducing the pressure (reducing the Rayleigh number) [2], by appropriate placement of the substrates (inclining the substrate with non-zero ψ, Fig. 1(a)) [8], by controlling the boundary conditions of the walls [3], and by adjustment of the system geometry [3].

This paper studies the mixed convection from a heated inclined plate inside a horizontal channel, a problem which is used to simulate the fluid dynamics and transport phenomena in chemical vapor deposition in a horizontal reactor with an inclined substrate. It also finds important applications in electronic cooling, where the plate is taken as an electronic component to be cooled. Since boundary conditions on the wall are critical to the uniformity of the transfer rate on the surface of the plate, several conditions on the wall are also examined. The initiation of the transverse rolls (local circulation) and their suppression by forced convection are investigated at various combinations of Rayleigh and Reynolds numbers and at different inclination angles and offsets.

MATHEMATICAL AND NUMERICAL FORMULATIONS

Coordinate considerations

When the inclination angle $\psi = 90°$ and the bottom surface is the substrate, the problem can be solved in Cartesian coordinates [3–6]. Since transverse rolls are suppressed by the forced convection in this situation, the equations are parabolized along the x-direction, so that only the y–z (the direction out of the paper) plane needs to be considered. The inclination of the plate, however, will suppress the longitudinal rolls (with axes upslope), but promote the transverse rolls, so that equations are elliptic in the x-direction due to local recirculation zones. From this point of view, we assume that the z-direction is long enough so that

† Present address: CFD Research Corporation, Huntsville, AL 35805, U.S.A.

NOMENCLATURE

c_{pm}	mean specific heat	u_0	characteristic velocity
g^{ij}, g_{ij}	contra-covariant metric tensors, respectively	u^i	contravariant velocity components ($i = 1, 2$)
G^i	gravitational acceleration vector ($i = 1, 2$)	W	channel width of calculation domain
h	heat transfer coefficient through the boundary wall	x, y	Cartesian coordinates.
h^*	dimensionless h, hH/k	Greek symbols	
H	height of channel	α	thermal diffusivity
H_1	offset height	β	volume expansion coefficient
k	thermal conductivity	δ_{ij}	Kronecker's delta
L	length of plate	θ^i	skewed coordinates ($i = 1, 2$)
n	unit normal vector	μ	dynamic viscosity
Nu	Nusselt number (equation (19))	ρ	density
p	static pressure	σ^{ij}	shear stress tensor
Pr	Prandtl number, $\mu/(\rho\alpha)$	Φ	dissipation function
q^i	conduction heat flux ($i = 1, 2$)	ψ	skewed angle along the x-axis
Ra	Rayleigh number, $\rho g\beta(T_H - T_C)H^3/(\mu\alpha)$	Subscripts	
Re	Reynolds number, $\rho u_0 H/\mu$	C	cold wall
S	source term	H	on the plate
T	temperature	t	time derivative
			spatial derivative.

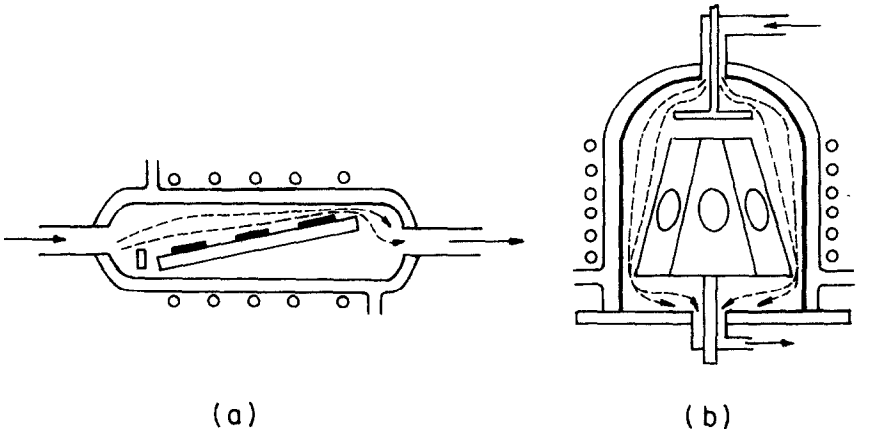

FIG. 1. Horizontal (a) and vertical (b) chemical vapor deposition reactors.

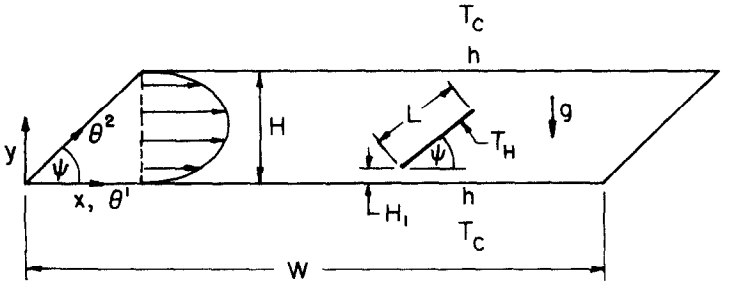

FIG. 2. Channel and plate geometry.

most of the flow is two-dimensional, in the sense that it varies only in the x–y plane. This assumption holds in the region away from the lateral walls, and in the angle range of $\psi > 30°$ in which longitudinal rolls do not initiate [9]. On the other hand, the inclination of the plate complicates the problem in that the traditional Cartesian coordinate system cannot be easily incorporated unless extensive modifications on the plate boundaries are made. The use of body-fitted coordinates can simplify the treatment of boundary conditions, but it introduces complexity in the governing equations, because they have to be transformed to the new coordinates. The orthogonal coordinates could be used as suggested by conformal mapping [10]. For the present geometry this will require large nonuniformity in the grid sizes [10]. A finite element technique can be used to solve the problem, but it is probably more expedient to utilize the skewed coordinates, by which one coordinate line is parallel to the plate and the other one is parallel to the channel walls as shown in Fig. 2. The advantages are that the governing equations take a relatively simple form as will be shown and boundary conditions can be readily specified.

Governing equations

In problems with complex geometries, it is usually the case that either the governing differential equations are accompanied by complex boundary conditions, or with simple boundary conditions, the forms of the governing equations become more complex. Fortunately, the governing equations in skewed coordinates still have relatively simple forms, and they have been recently shown for the three-dimensional arbitrary parallelepiped geometry [11]. Basically, the governing equations are transformed from the Cartesian coordinates to the curvilinear non-orthogonal coordinates. The present skewed coordinates (θ^1, θ^2) have the property that they are linearly related to the Cartesian coordinates (x, y) as shown in Fig. 2. By this property, a simple set of equations is obtained as follows

$$\rho_t + (\rho u^i)_{,i} = 0 \tag{1}$$

$$(\rho u^i)_t + (\rho u^i u^j)_{,j} = -p_{,j} g^{ij} + \rho G^j + (\sigma^{ij})_{,j} \tag{2}$$

$$(\rho c_{pm} T)_t + (\rho c_{pm} u^i T)_{,i} = (k T_{,j} g^{ij})_{,i} + \mu\Phi - p u^i_{,i} \tag{3}$$

$$\sigma^{ij} = \mu(u^j_{,m} g^{mi} + u^j_{,m} g^{mj} - 2/3 \delta^{ij} u^m_{,m}) \tag{4}$$

$$\Phi = 2[(u^i_{,j})^2]\delta^j_i + [u^i_{,j}(1-\delta^j_i)]^2 - 2/3(u^i_{,i})^2. \tag{5}$$

All the symbols are defined in the Nomenclature. It is to be noted that the derivatives ',i' are with respect to θ^i. These equations are almost in the same form as those in Cartesian coordinates, except the terms involving the first derivatives of the scalars or vectors (not the tensors), such as $p_{,j} g^{ij}$, $T_{,j} g^{ij}$ and $u^j_{,m} g^{mi}$. As for the present problem, the contravariant metric tensor, g^{ij}, which plays an essential role in the solution, can be easily found through the coordinate relations as

$$g^{11} = 1/\sin^2\psi$$

$$g^{12} = g^{21} = -\cos\psi/\sin^2\psi$$

$$g^{22} = 1/\sin^2\psi. \tag{6}$$

When $\psi = 90°$, $g^{ij} = \delta^{ij}$, and equations (1)–(5) return to those in Cartesian coordinates.

Boundary conditions

In the inlet region flow is assumed to be fully developed. The upper and lower walls are subject to exterior heat losses with a heat transfer coefficient h to the ambient, which has the same temperature as the inlet fluid, T_C. At the outlet, all the derivatives of the dependent variables along the θ^1-direction are zero. Thus, we have

$$\theta^1 = 0, \quad u^1 = 6u_0[1-(\theta^2 \sin\psi/H)]\theta^2 \sin\psi/H$$

$$u^2 = 0, \; T = T_C \tag{7}$$

$$\theta^1 = W, \quad (u^1)_{,1} = 0, \; (u^2)_{,1} = 0$$

$$(T)_{,1} = 0 \tag{8}$$

$$\theta^2 = 0, \quad q^2 \sin\psi = -h(T_w - T_C)$$

$$u^1 = u^2 = 0 \tag{9}$$

$$\theta^2 = H/\sin\psi, \quad q^2 \sin\psi = h(T_w - T_C)$$

$$u^1 = u^2 = 0. \tag{10}$$

Here T_w is the unknown temperature at the wall, and q^2 the contravariant component of the conduction heat flux

$$q^2 = kT_{,2} g^{22} + kT_{,1} g^{12}. \tag{11}$$

The sine quantities in q^2 of equations (9) and (10) come from the decomposition of the heat flux vector into the direction normal to the walls.

The temperature of the plate is held at T_H, while velocity components are zero, i.e. in the plate

$$T = T_H, \; u^1 = u^2 = 0. \tag{12}$$

Finite difference equation and the solution

The methodology to solve equations (1)–(3) has been described in detail in ref. [11]. What is done is to separate those terms due to nonorthogonality into two parts, so that

$$-q^i = kT_{,j} g^{ij} = kT_{,i} g^{ii} + (kT_{,j} g^{ij} - kT_{,i} g^{ii}) \tag{13}$$

and the term in parentheses is grouped into the source term and treated as known from the last iteration. In this way, the energy equation (3) becomes

$$(\rho c_{pm} T)_t + (\rho c_{pm} u^i T)_{,i} = (kT_{,i} g^{ii})_{,i} + S \tag{14}$$

where

$$S = \mu\Phi - p u^i_{,i} + \sum_{i,j} (kT_{,j} g^{ij} - kT_{,i} g^{ii})_{,i}. \tag{15}$$

Equation (14) is in the same form as that in Cartesian coordinates, and the algorithm by Patankar [12] can

be applied directly. However, it is noted that the coefficient g^{ij} appears in the conduction term. Similar modifications also apply to the momentum equation (2)

$$p_{,i}g^{ij} = p_{,i}g^{ij} + (p_{,j}g^{ij} - p_{,i}g^{ij}) \tag{16}$$

$$\sigma^{ij} = \mu u^i_{,j} + (\sigma^{ij} - \mu u^i_{,j}). \tag{17}$$

Here again, the link coefficient in the pressure correction equation [12] has to be modified due to g^{ij}. This methodology has been found to be successful in dealing with natural convection in arbitrary three-dimensional parallelpiped enclosures [11].

RESULTS AND DISCUSSIONS

There are several parameters controlling the transport phenomena in the channel. These are the Rayleigh number, Ra; the Prandtl number, Pr; the Reynolds number, Re; the aspect ratio of the calculation domain, W/H; the inclination angle, ψ; the plate offset position, H_1, and its length, L; and the heat transfer coefficient from the boundary wall h. Since physical properties are included in some parameters, they are evaluated at the inlet temperature and kept constant. The following definitions are utilized:

$$\left.\begin{aligned} Ra &= \rho g\beta(T_H - T_C)H^3/(\mu\alpha) \\ Re &= \rho u_0 H/\mu \\ Pr &= \mu/(\rho\alpha) \\ h^* &= hH/k. \end{aligned}\right\} \tag{18}$$

It is difficult to exhaust the whole range of parameters, instead, we fix Ra at 5.2×10^3 which is above the highest value in other studies [3–6], while Re is varied from 1.2×10^{-1} to 1.2×10^2 to cover the range from the natural-convection dominant flow to the forced-convection dominant flow. The plate length is fixed at $L = 0.54H$ and its relative position H_1 (Fig. 2) is varied from 0 to $0.4H$. The inclination angle ψ is taken to be at 60° and 120° to determine the aiding and opposing effects of the forced convection [9]. It is pointed out here that in the numerical calculation, convergence is much faster in the angle range close to 90° than at other angles. Convergent results are obtainable in the angle range from 30° to 150°. The dimensionless heat transfer coefficient on the outside of the wall, h^*, varies from zero to infinity to cover the adiabatic as well as the isothermal boundary conditions.

Validation study

The pure forced convection with developing flow in a channel, where the plate is absent and $\psi = 90°$, is first used for validation, since the analytical solution is available. Comparisons in the temperature, velocity and heat transfer rate between the numerical and analytical results are found to be very good. Comparison with experimental data for a parallelpiped has been documented in ref. [11].

The computational domain and grid are also very important issues. In general, the domain should be properly selected so that the dependent variables at the inlet and outlet are not effected by the circulation regions near the plate. An aspect ratio $W/H = 6.0$ is found to be suitable for the parameter ranges considered here. The length upstream of the plate depends on the size of the recirculation zone driven by natural convection, while the length downstream of the plate depends on the forced convection in order to satisfy boundary conditions (8). To have better resolution of the local variation of the temperature and velocities near the plate, the grids are distributed nonuniformly in the θ^1 coordinates, but uniformly in the θ^2 coordinates, so that more calculation cells are located near the plate and less grids are in the inlet and outlet regions. This arrangement is by an exponential distribution of the grid sizes. A non-uniformly distributed 90×30 ($\theta^1\times\theta^2$) cell system is shown in Fig. 3. Actually, several grid systems have been tested for the limiting cases of $Ra = 5.2\times10^3$, $Re = 1.2\times10^{-1}$ and $Re = 1.2\times10^2$, with $H_1 = 0.13H$, $\psi = 60°$ and $h^* = \infty$. In Fig. 4 the local variations of the Nusselt number are plotted for various cell systems. Here the Nusselt number is defined as

$$Nu = H\nabla T\cdot\mathbf{n}/(T_H - T_C) \tag{19}$$

where $\mathbf{n}$ is the unit vector normal to the plate, ∇T the temperature gradient, and H the height of the channel. This Nusselt number is different from the h^* defined in ref. [18] in that, here Nu is for the plate, while h^* is for the wall. The average Nusselt number over the plate is shown in Table 1. It is seen that the two non-uniform grid systems of $90\times30^*$ and $90\times45^*$ cells give results very close to each other, and the grid of $90\times30^*$ is used in all subsequent calculations.

The calculations are carried out on an IBM 3033 mainframe. A typical run to reach steady state for $90\times30^*$ cells takes about 40 min CPU time covering 1500 time steps.

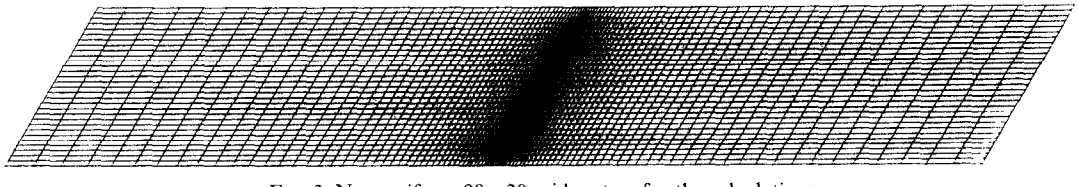

FIG. 3. Non-uniform 90×30 grid system for the calculations.

Table 1. Comparison of Nusselt number at several grids for $Ra = 5.2 \times 10^3$

	90×15	90×30	90×45	90×30*	90×45*
$Re = 1.2 \times 10^{-1}$	4.903	4.530	4.617	4.586	4.522
$Re = 1.2 \times 10^{2}$	14.58	15.83	16.46	16.74	16.87

*Exponential non-uniform cells in the θ^1-direction.

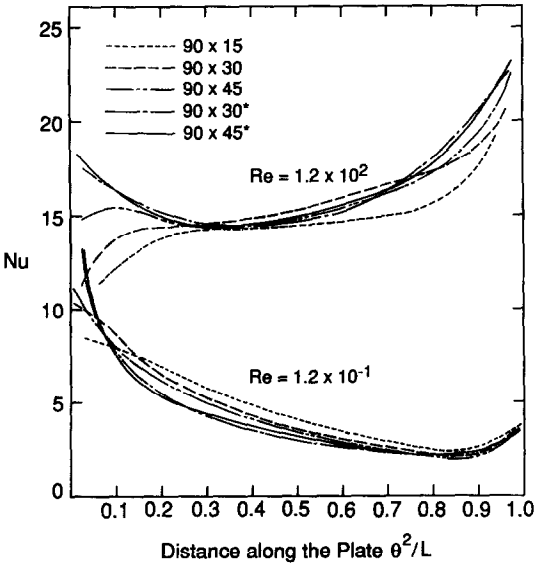

FIG. 4. Local heat transfer rate along the plate on the upward-facing side at $H_1 = 0.13H$, $\psi = 60°$, $h = \infty$ with several grid systems.

Natural-convection to forced-convection dominant flows

First the calculations are for the case with $H_1 = 0$, $h^* = 0$ (adiabatic wall), $\psi = 60°$ but varying Reynolds number to examine the impact of forced convection on the natural convection from the plate. Figures 5 and 6 show the isotherms and streamlines, respectively, with increasing Reynolds numbers. Figure 5(a) displays the isotherms for $Re = 1.2 \times 10^{-1}$ ($Ra/Re^2 = 3.6 \times 10^5$). It is a typical motion dominated by natural convection. The fluid particles close to the plate are heated up so that they move up along the plate due to the buoyancy force. Different from the motion in an infinite medium, the restriction of the two channel walls gives rise to local circulation zones as shown in Fig. 6(a). As the plate is inclined the buoyancy force has two components, one is tangent to the plate which drives the flow, and the other is perpendicular to the plate. The latter has different effects on the two sides. For the upward-facing side, it tends to destabilize and separate the boundary layer formed along the plate, a fact which has been observed experimentally by Fujii and Imura [13] and by Moran and Lloyd [14]. The perpendicular component of the buoyancy force, however, tends to stabilize the flow on the downward-facing side. This point can be well understood from the isotherms on the two sides of the plate, which show different trends with increasing θ^2. On the upward-facing side, isotherms become less dense, and on the downward-facing side, they become more dense. These facts lead to a decrease in heat transfer rate along the upward-facing side of the plate and an increase along the downward-facing side. The small heat transfer rate at the bottom edge of the downward-facing plate is due to almost stagnant flow there.

On the other hand, the buoyancy force component perpendicular to the plate tends to accelerate the circulation motion in the upward-facing surface side, and decelerate that on the downward-facing side as shown by the maximum stream-function values on the two sides of the plate in Fig. 6(a).

At $Re = 1.2 \times 10^0$ (or $Ra/Re^2 = 3.6 \times 10^3$), forced convection starts to exert its effects as may be seen from the streamlines in Fig. 6(b). This forced convection flow has an aiding effect on the flow above the upward-facing plate. The isotherms in Fig. 5(b) seem unchanged, compared to those in Fig. 5(a). Careful examination, however, reveals that near the upward-facing side isotherms become denser and the fluid motion gets stronger as indicated by the value of the streamfunctions in Fig. 6(b). A further increase of Re in Fig. 6(c) ($Re = 3.8 \times 10^1$, $Ra/Re^2 = 3.6 \times 10^2$) repels the circulation cells away from the plate and the deformation of the isotherms becomes more severe, with more dense isotherms on the upward-facing side and less dense ones on the downward-facing side. At $Re = 1.2 \times 10^1$ or $Ra/Re^2 = 3.6 \times 10^1$, as seen in Fig. 6(d), the circulation cells due to natural convection become weaker, and are finally washed out. The streamlines show clearly that the control mechanism is forced convection. When the flow is further dominated by forced convection in Figs. 5(e) and 6(e) ($Re = 1.2 \times 10^2$, $Ra/Re^2 = 3.6 \times 10^{-1}$) the isotherms accumulate on the upward-facing side, while separation occurs behind the plate.

Figure 7 shows the local heat transfer coefficient Nu. As predicted from isotherms, the heat transfer rate on the downward-facing plate displays a gradual increase along the plate when natural convection is dominant, while the heat transfer on the upward-facing side displays a gradual decrease. It is interesting to note that the increase in Reynolds number leads to a dramatical change in heat transfer rate on the upward-facing side. When forced convection is dominant the heat transfer rate on the upper side of the plate increases along the direction of increasing θ^2, but with a level much higher than that on the lower

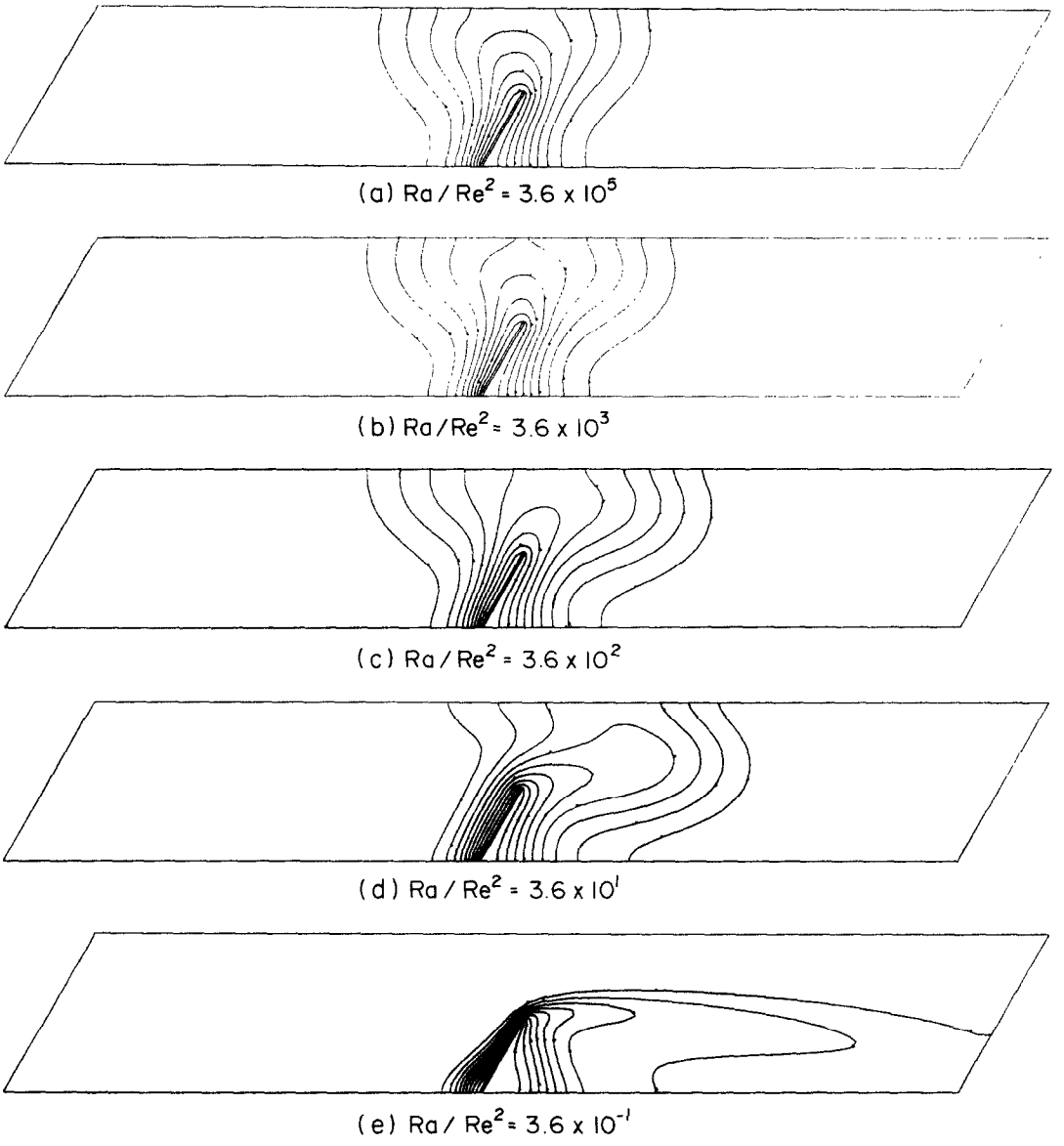

FIG. 5. Isotherms at $Ra = 5.2 \times 10^3$, $Pr = 0.71$, $\psi = 60°$, $H_1 = 0$, $h^* = 0$ and various Reynolds numbers.

side of the plate. It can be seen that with the increase of Reynolds number, the slope of the Nusselt number along the plate changes, and at a certain combination of Rayleigh number and Reynolds number ($Ra/Re^2 = 3.6 \times 10^1$ here), an almost uniform heat transfer along the plate can be obtained on the upward-facing side. This is due to the fact that Rayleigh number and Reynolds number have opposite effects on the Nusselt number distribution along the upside of the plate. Figure 8 shows the variations of dimensionless temperature $(T-T_C)/(T_H-T_C)$ with θ^1, which shows a typical boundary layer characteristic when Reynolds number increases.

Influence of inclination angle and offsets

Similar computations have been made for an inclination angle of 120°, $h^* = \infty$ (isothermal boundary walls) and offsets of $H_1 = 0.13H$ and $0.4H$ to reveal the interaction of forced convection and natural convection. The results for both inclination angles in terms of isotherms and streamlines are displayed in Figs. 9–12. Geometrically, the four configurations can be recovered from any one of them by simply rotating the whole structure over 180° along the θ^1-axis, an action changing the influence of the natural convection; or by supplying forced flow in the negative θ^1-directions, an action changing the influence of forced convection. The resulting interactions, however, are quite different, as will be seen. In Figs. 9–12, (a) is the case for $Ra/Re^2 = 3.6 \times 10^3$, which is the starting point of the forced convection having an effect on natural convection; and (b) is the case for $Ra/Re^2 = 3.6 \times 10^1$, where a nearly uniform heat transfer rate at $\psi = 60°$, $H_1 = 0$ and $h^* = 0$ is obtained.

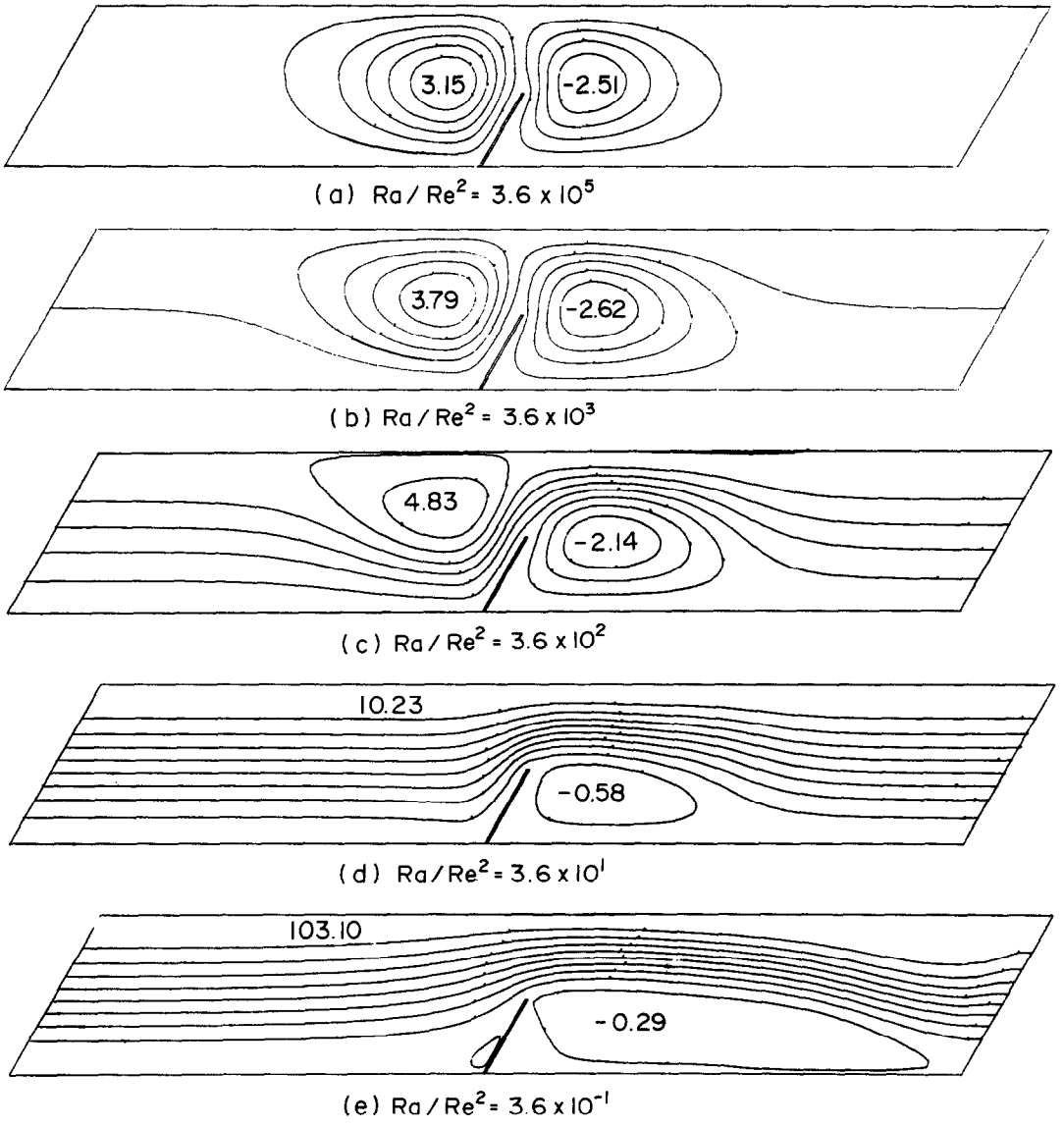

FIG. 6. Streamlines at $Ra = 5.2 \times 10^3$, $Pr = 0.71$, $\psi = 60°$, $H_1 = 0$, $h^* = 0$ and various Reynolds numbers.

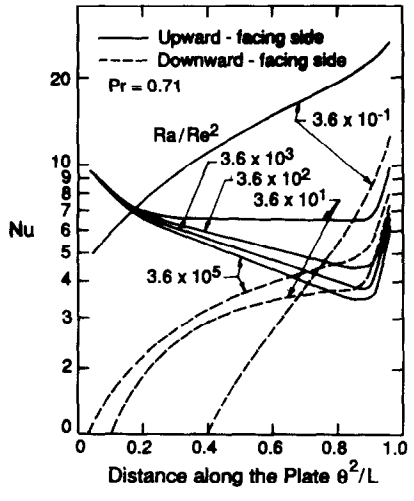

FIG. 7. Local heat transfer rate at $Ra = 5.2 \times 10^3$, $Pr = 0.71$, $\psi = 60°$, $H_1 = 0$, $h^* = 0$ and various Reynolds numbers.

In Fig. 9(a), $\psi = 60°$ but $H_1 = 0.13H$, the isotherms show a stratification above the plate, which is unstable up to a certain Rayleigh number (about 10^4 in the present study), thus leading to the formation of a thermal plume. Different from the one in Fig. 5(b) with the same Rayleigh and Reynolds numbers, the isotherms here accumulate along the downward-facing side almost uniformly. This is partly due to the 'leaking' of the fluid through the slot below the plate, which promotes the flow interaction between both sides of the plate. It is also due to the difference in boundary conditions (isothermal walls here). The forced convection is seen to start affecting the natural convection in the same way as that in Fig. 6(b). When $Ra/Re^2 = 3.6 \times 10^1$, as shown in Fig. 9(b), we see deformed isotherms, and the disappearance of the convection cell on the upside of the plate. There is still a small convection cell on the lower side of the plate and leakage of the forced flow between the plate can

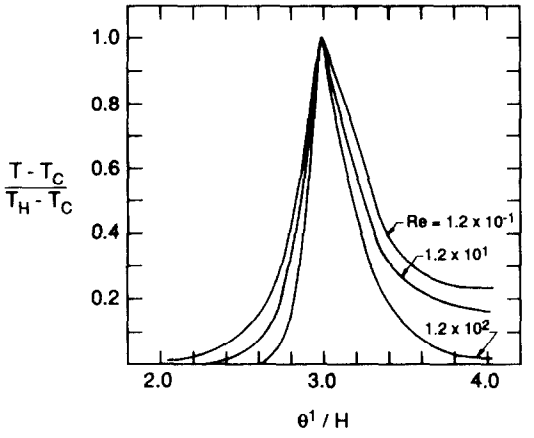

FIG. 8. Dimensionless temperature along the θ^1-direction at half height of the plate at $Ra = 5.2 \times 10^3$, $Pr = 0.71$, $\psi = 60°$, $H_1 = 0$, $h^* = 0$.

also be observed. The distribution of the local Nusselt number for Fig. 9(b) is shown in Fig. 13 and we still note a uniform heat transfer distribution in the central region of the plate. Here the higher Nusselt number near the two ends of the plate is due to the edge effect as a result of the isothermal wall on both sides. When the inclination angle becomes 120° (Fig. 10(a)), interestingly, we see the forced convection streamlines dividing around the plate due to the increasing pressure along the upstream side (or downward-facing side). When *Re* is increased, a stagnant region occurs behind the plate, which results in a small heat transfer rate for the plate on that side. That on the upstream side of the plate, however, is still uniform but slightly lower than that at $\psi = 60°$. When the plate is tilted at $\psi = 60°$ with $H_1 = 0.4H$ (Fig. 11(a)), the forced convection affects the natural convection from the downward-facing side, which is different from the one in Fig. 9(a). At a higher Rayleigh number (Fig. 11(a)), forced convection has an opposing effect on the natural convection at the upside of the plate. The intensity of forced convection is not that high, thus leaving a relative stagnant region there and the heat transfer rate is no longer uniform as shown in Fig. 13 and is at a lower level. With an inclination angle of 120° (Fig. 12(a)) the forced convection effect starts from the bottom of the plate and finally all the flow passes

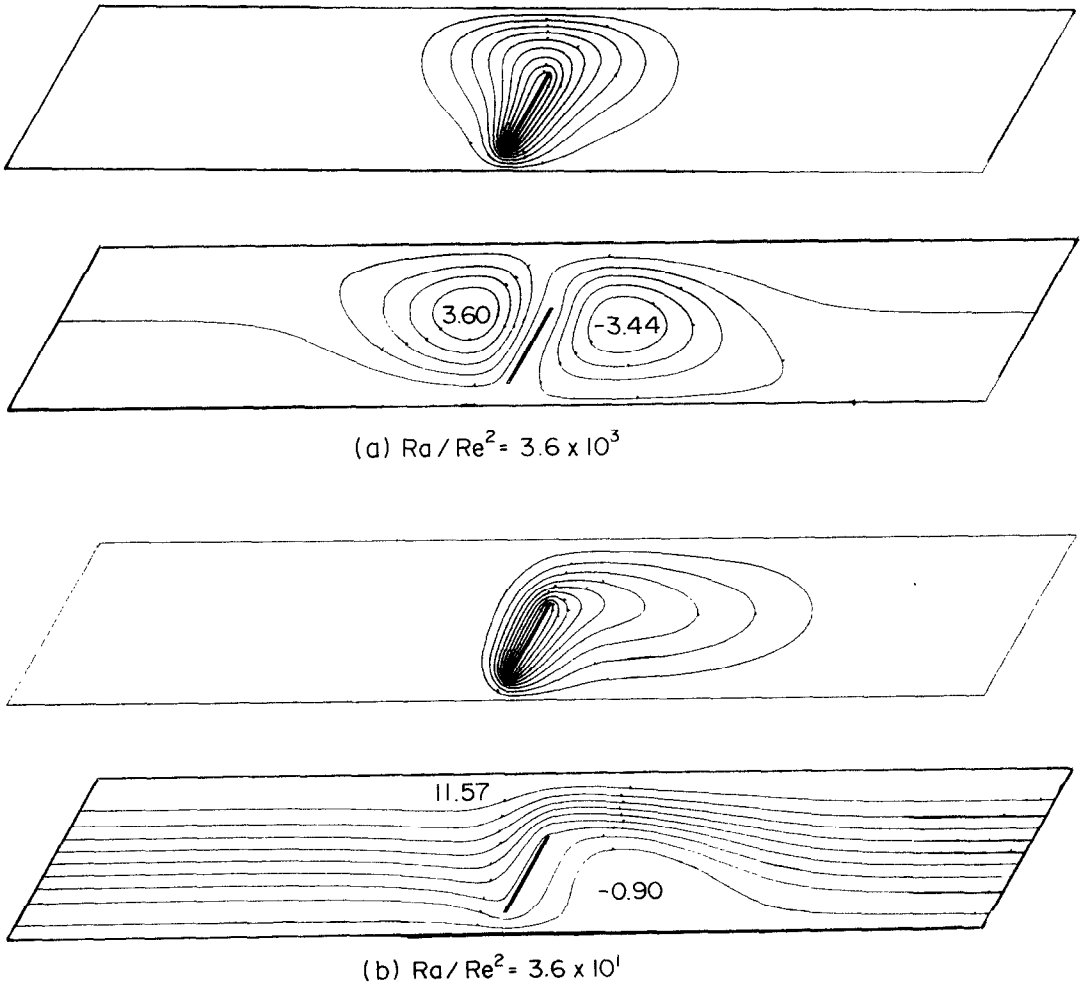

FIG. 9. Isotherms and streamlines at $Ra = 5.2 \times 10^3$, $\psi = 60°$, $H_1 = 0.13H$, $h^* = \infty$: (a) $Ra/Re^2 = 3.6 \times 10^3$; (b) $Ra/Re^2 = 3.6 \times 10^1$.

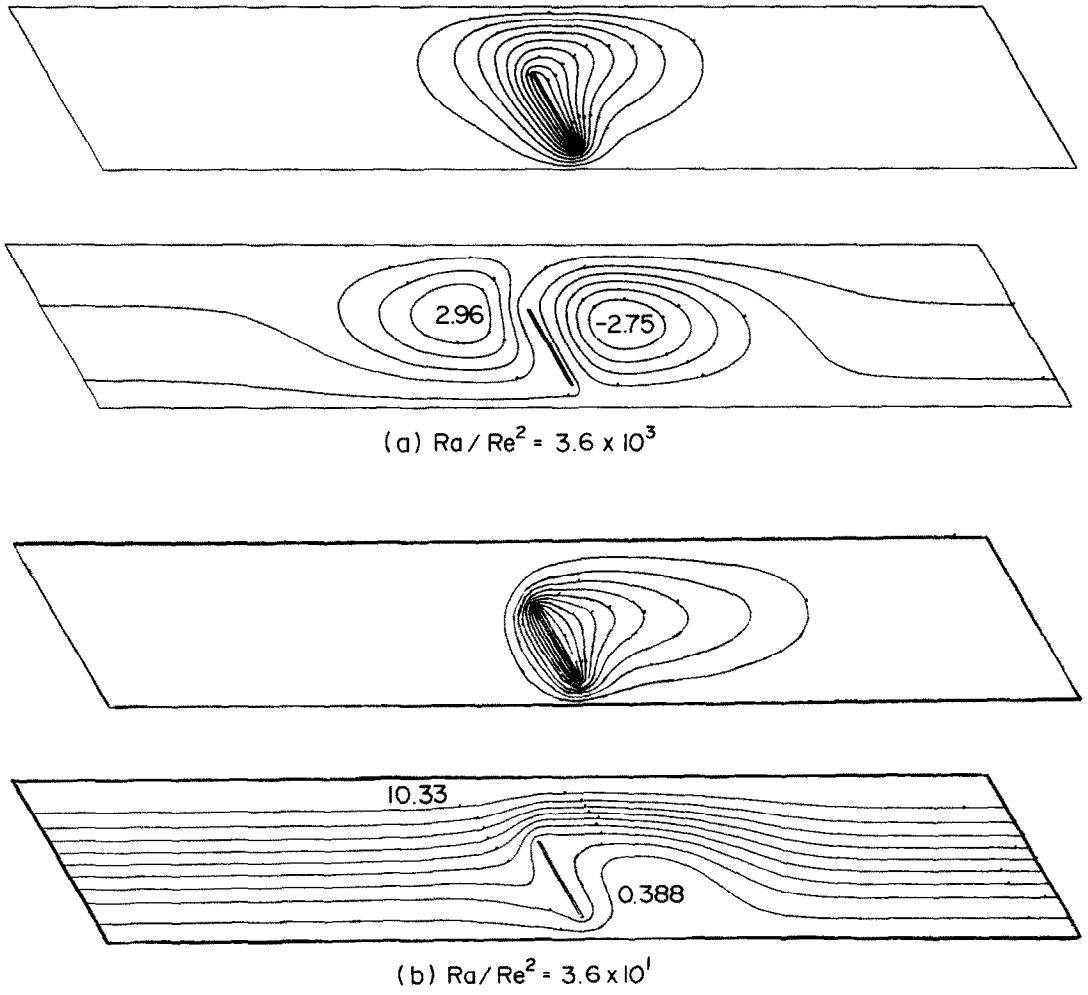

FIG. 10. Isotherms and streamlines at $Ra = 5.2 \times 10^3$, $\psi = 120°$, $H_1 = 0.13H$, $h^* = \infty$: (a) $Ra/Re^2 = 3.6 \times 10^3$; (b) $Ra/Re^2 = 3.6 \times 10^1$.

there (Fig. 12(a)). Even though the forced convection has an opposing effect, it is much more dominant so that the heat transfer rate shows some uniformity (Fig. 13).

Influence of the boundary conditions

In the usual CVD process, the boundary walls are kept at a constant lower temperature to avoid unnecessary deposition on the wall [3]. This condition, however, promotes the buoyant flow, when $\psi = 90°$ and the bottom wall is taken as the substrate and is heated [3–6]. It remains to see what happens when the substrate is inclined. The centrally located plate at $\psi = 60°$ with various dimensionless heat transfer rates h^* through the boundary walls is considered, for $Re = 1.2 \times 10^{-1}$ and 1.2×10^1, both with $Ra = 5.2 \times 10^3$. Since streamlines are not much different from the other cases, only isotherms are displayed in Figs. 14 and 15. With the lower h^* (nearly adiabatic boundary), the walls are heated to a higher temperature. In both cases, the basic feature is that the isotherms spread widely at the low h^* and gradually squeeze together with increasing h^*. The dimensionless heat transfer through the boundary wall h^* has pronounced influences on the heat transfer from the plate at low Reynolds number situations as seen from Fig. 16, which shows the local heat transfer rate from the plate. Once forced convection becomes important, however, the variation of heat transfer rate for the plate with h^* becomes much less sensitive. Physically, the deformation of isotherms can be understood as that, at low h^*, energy is mostly transferred to the outlet, while at higher h^* it is mostly transferred through the wall regions, so as to leave an almost uniform and lower temperature outlet region there. In Fig. 17, the average heat transfer from the plate at various h^* is shown. It is seen that h^* indeed has a pronounced influence on the natural convection dominant case.

CONCLUDING REMARKS

The influence of forced convection on the natural convection from an inclined, heated plate, which is

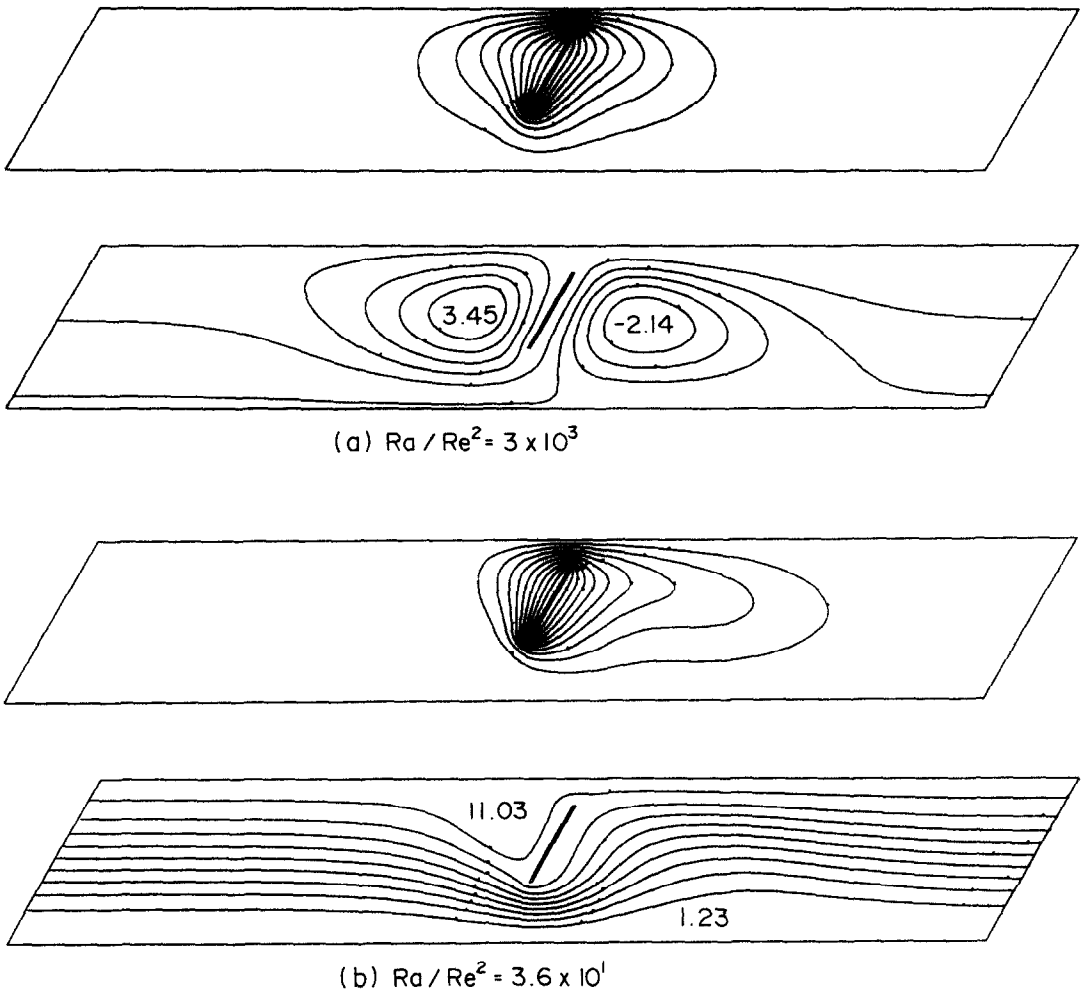

FIG. 11. Isotherms and streamlines at $Ra = 5.2 \times 10^3, \psi = 60^\circ, H_1 = 0.4H, h^* = \infty$: (a) $Ra/Re^2 = 3.6 \times 10^3$; (b) $Ra/Re^2 = 3.6 \times 10^1$.

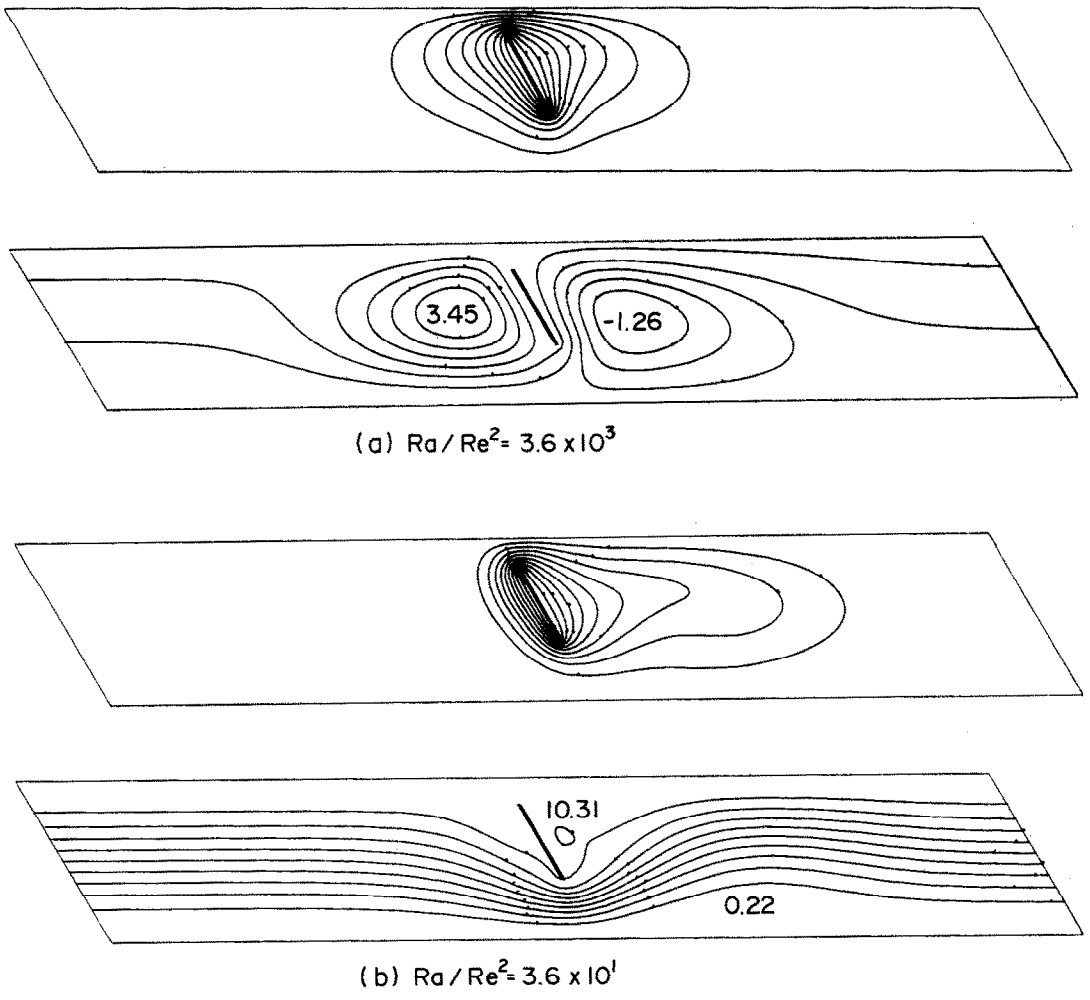

FIG. 12. Isotherms and streamlines at $Ra = 5.2 \times 10^3$, $\psi = 120°$, $H_1 = 0.4H$, $h^* = \infty$: (a) $Re = 1.2 \times 10^0$; (b) $Re = 1.2 \times 10^1$.

taken as the substrate in a CVD process inside a horizontal channel is studied numerically. The solutions are based on skewed coordinates with one coordinate line parallel to the channel wall and another one parallel to the plate, which makes the treatment of the boundary condition easier. The primary study is on a fixed Rayleigh number with varying Reynolds numbers, inclination angles, offsets and boundary conditions. When the flow is natural convection dominant, local circulation zones (transverse roll cells) are generated due to the presence of the channel wall, which gives rise to nonuniformity in the transfer rate from the plate. However, by increasing forced flow this can be greatly improved, and at a certain combination of Rayleigh and Reynolds numbers a uniform heat transfer can be obtained. The offset and inclination angle of the plate may also alter the nature of the interaction of forced and natural convection. A wall with high heat transfer to the ambient will promote the natural convection but has little influence when the forced convection is important.

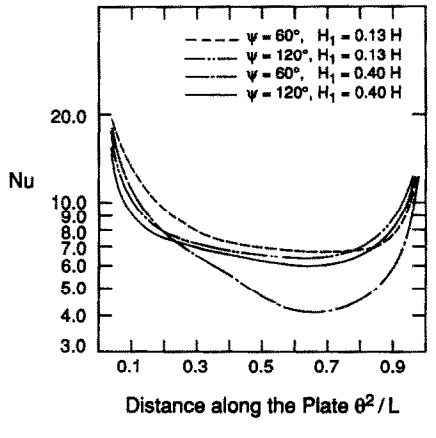

FIG. 13. Local heat transfer rate along the upstream side of the plate at $Ra = 5.2 \times 10^3$, $Re = 1.2 \times 10^1$, $h^* = \infty$, with several ψ and H_1.

In real CVD applications, the mass transfer, variable physical properties, radiation, and more complicated geometries need to be included. Nevertheless, the present study provides certain insight into the interaction of natural convection and forced convection in CVD like geometries. Further study with

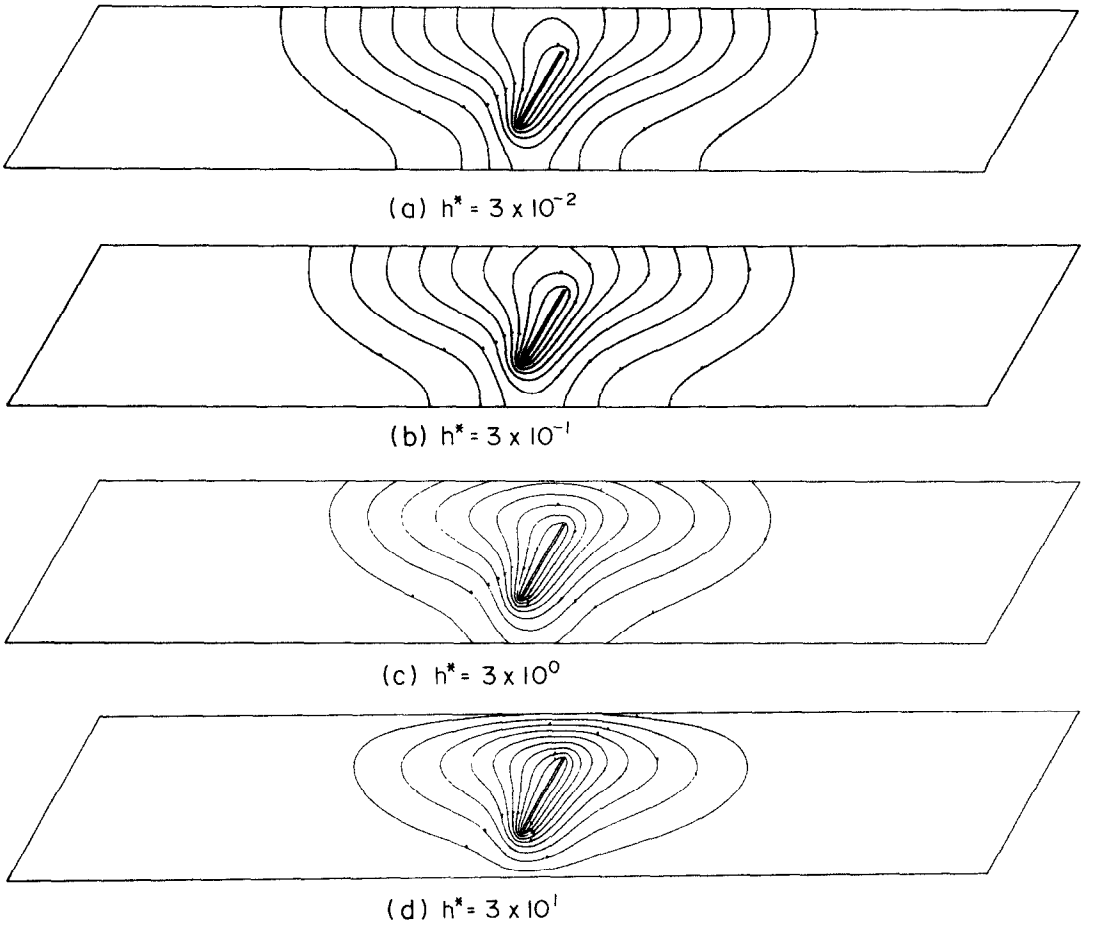

FIG. 14. Isotherms and streamlines at $Ra = 5.2 \times 10^3$, $\psi = 60$, $Re = 1.2 \times 10^{-1}$ and various h^*.

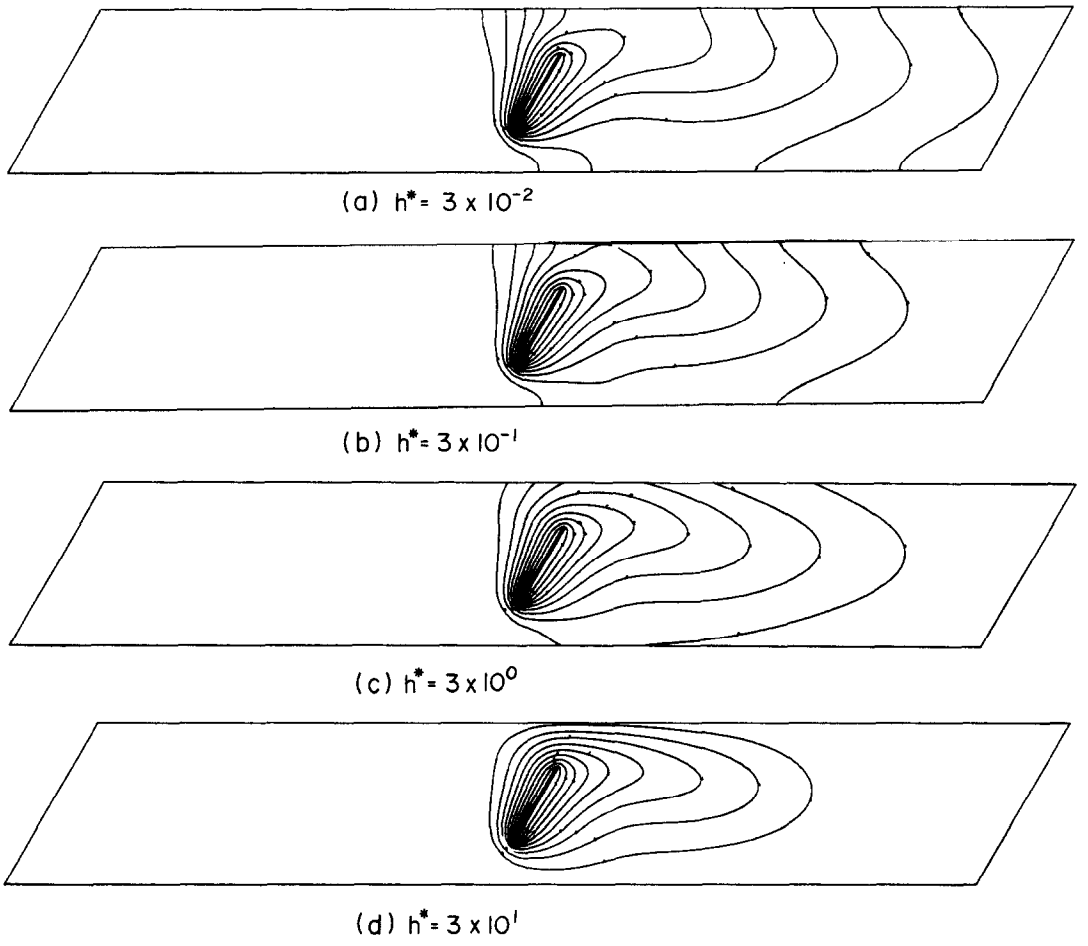

FIG. 15. Isotherms and streamlines at $Ra = 5.2 \times 10^3$, $\psi = 60°$, $Re = 1.2 \times 10^1$ and various h^*.

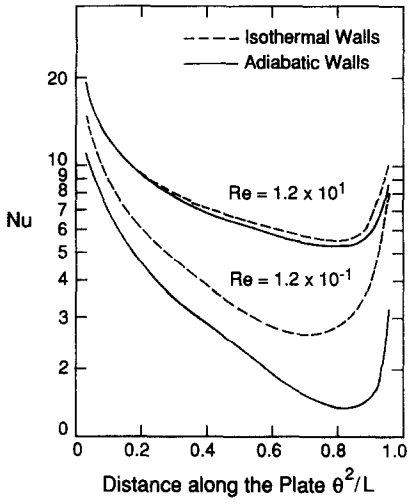

FIG. 16. Boundary effects on the local Nusselt number on the upward-facing side at $Ra = 5.2 \times 10^3$, $H_1 = 0.26H$ and $\psi = 60°$.

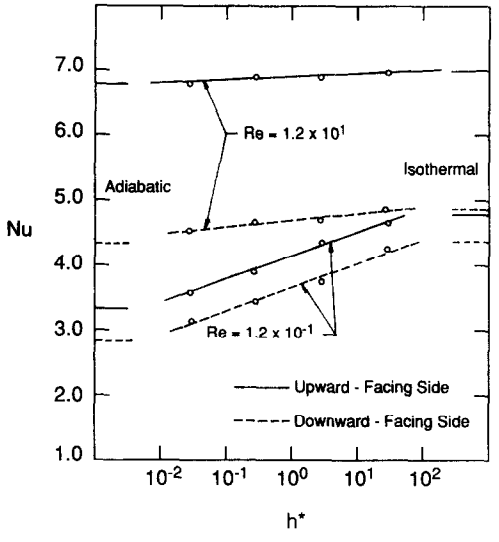

FIG. 17. Boundary effects on the average Nusselt number at $Ra = 5.2 \times 10^3$, $H_1 = 0.26H$ and $\psi = 60°$.

consideration of the above parameters has been initiated.

REFERENCES

1. F. Rosenberger, Fluid dynamics in crystal growth from vapors, *PhysicoChem. Hydrodyn.* **1**, 1–24 (1979).
2. S. Ostrach, Fluid mechanics in crystal growth—The 1982 Freeman Scholar Lecture, *J. Fluid Engng* **105**, 5–20 (1983).
3. K. F. Jensen, D. I. Fotiadis, H. K. Moffat, E. O. Einset, A. M. Kremer and D. R. McKenna, Fluid mechanics of chemical vapor deposition. In *Interdisciplinary Issues in Materials Processing and Manufacturing* (Edited by S. K. Samanta *et al.*), Vol. 2, pp. 565–585. ASME, New York (1987).
4. K. C. Chiu and F. Rosenberger, Mixed convection between horizontal plates—I. Entrance effects, *Int. J. Heat Mass Transfer* **30**, 1645–1654 (1987).
5. K. C. Chiu, J. Ouazzani and F. Rosenberger, Mixed convection between horizontal plates—II. Fully developed flow, *Int. J. Heat Mass Transfer* **30**, 1655–1662 (1987).
6. S. Rhee, J. Szekely and O. J. Iiegbusi, On three-dimensional transport phenomena in CVD processes, *J. Electrochem. Soc.* **134**, 2552–2559 (1987).
7. F. P. Incropera and J. A. Schutt, Numerical simulation of laminar mixed convection in the entrance region of horizontal rectangular ducts, *Numer. Heat Transfer* **8**, 707–729 (1985).
8. G. B. Stringfellow, Vapor phase growth. In *Crystal Growth* (Edited by B. R. Pamplin), pp. 181–274. Pergamon Press, Oxford (1980).
9. T. S. Chen and B. F. Armaly, Mixed convection in external flow. In *Handbook of Single-phase Convective Heat Transfer* (Edited by S. Kakac, R. K. Shah and W. Aung). Wiley, New York (1987).
10. G. Ryskin and L. G. Leal, Orthogonal mapping, *J. Comp. Phys.* **50**, 71–100 (1983).
11. H. Q. Yang, K. T. Yang and J. R. Lloyd, Buoyant flow calculations with non-orthogonal curvilinear coordinates for vertical and horizontal parallelepipeds, *Int. J. Numer. Meth. Engng* **25**, 331–345 (1988).
12. S. V. Patankar, *Numerical Heat Transfer and Fluid Flow*. Hemisphere, Washington, DC (1980).
13. T. Fujii and H. Imura, Natural convection heat transfer from a plate with arbitrary inclination, *Int. J. Heat Mass Transfer* **15**, 755–767 (1972).
14. W. R. Moran and J. R. Lloyd, Natural convection mass transfer adjacent to vertical and downward-facing surfaces, *ASME J. Heat Transfer*, Ser. C **97**, 472–474 (1975).

CONVECTION MIXTE SUR UNE PLAQUE INCLINEE CHAUDE DANS UN CANAL AVEC APPLICATION AU CVD

Résumé—Une étude numérique basée sur les équations descriptives dans des coordonnées obliques est faite pour déterminer l'influence de la convection forcée sur la convection naturelle pour une plaque inclinée et chaude, située dans un canal horizontal. La convection forcée augmente le transfert de chaleur aussi bien qu'elle rend le flux thermique plus uniforme sur la face tournée vers le haut. Les conditions aux limites, l'angle d'inclinaison et la position de fixation ont des effets sensibles sur l'intéraction des deux convections forcée et naturelle.

MISCHKONVEKTION AN EINER BEHEIZTEN GENEIGTEN PLATTE IN EINEM DURCHSTRÖMTEN KANAL

Zusammenfassung—Auf der Grundlage der Bilanzgleichungen in schiefen Koordinaten wird der Einfluß einer erzwungenen Konvektionsströmung auf die natürliche Konvektion an einer geneigten Heizfläche in einem waagerechten Kanal numerisch untersucht. Es wird herausgefunden, daß die erzwungene Konvektion den Wärmeübergang insgesamt verbessert und an der Oberseite der Platte gleichförmiger macht. Die Randbedingungen, der Neigungswinkel und die geometrische Anordnung haben einen signifikanten Einfluß auf das Zusammenwirken von erzwungener und natürlicher Konvektion.

СМЕШАННАЯ КОНВЕКЦИЯ ОТ НАГРЕТОЙ НАКЛОННОЙ ПЛАСТИНЫ В КАНАЛЕ

Аннотация—На основе определяющих уравнений в косоугольных координатах проведено численное исследование влияния вынужденной конвекции на естественную у наклонной нагретой пластины, расположенной внутри горизонтального канала. Найдено, что вынужденная конвекция усиливает теплоотдачу, а также способствует развитию более однородной интенсивности теплоотдачи на верхней стороне пластины. Установлено, что граничные условия, углы наклона и положение пластины оказывают значительное влияние на взаимодействие вынужденной и естественной конвекции.